CHEMISTRY
A European Journal

Supporting Information

A Unique Ln^{III}\{[3.3.1]Ga^{III} Metallacryptate\} Series That Possesses Properties of Slow Magnetic Relaxation and Visible/Near-Infrared Luminescence

Jacob C. Lutter,[a] Svetlana V. Eliseeva,*[b] Jeff W. Kampf,[a] Stéphane Petoud,*[b] and Vincent L. Pecoraro*[a]

chem_201801355_sm_miscellaneous_information.pdf

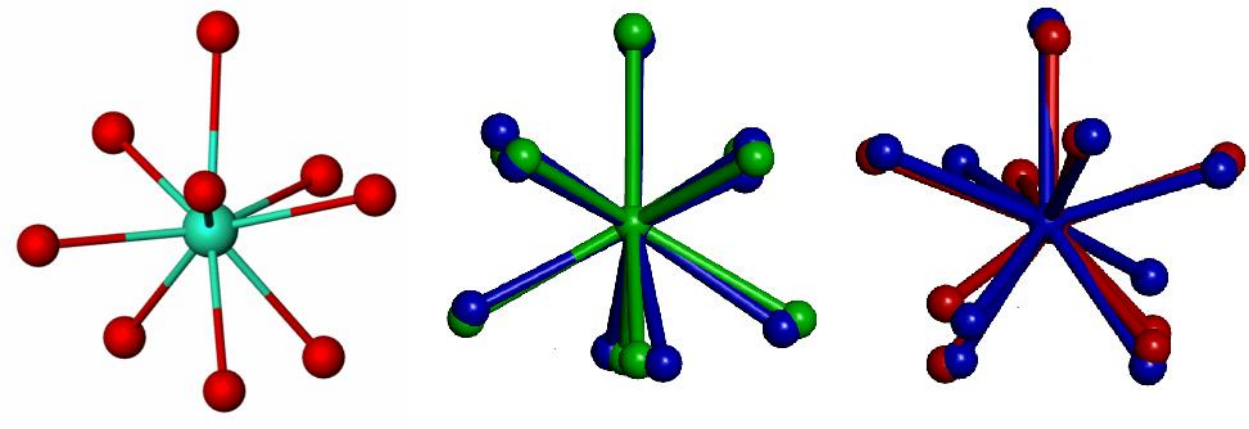

Figure S1. First coordination sphere of Tb1 in **Tb-1**, b) **Tb-1** (blue) overlaid with an ideal tricapped trigonal prism (green), c) **Tb-1** (blue) overlaid with an ideal monocapped square antiprism (red).

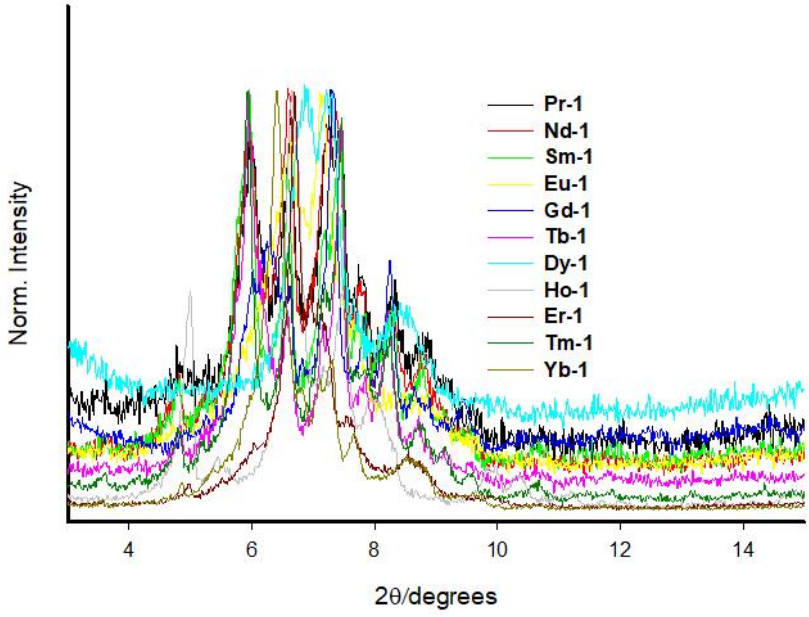

Figure S2a. Overlay of **Ln-1** PXRD spectra show nearly consistent composition.

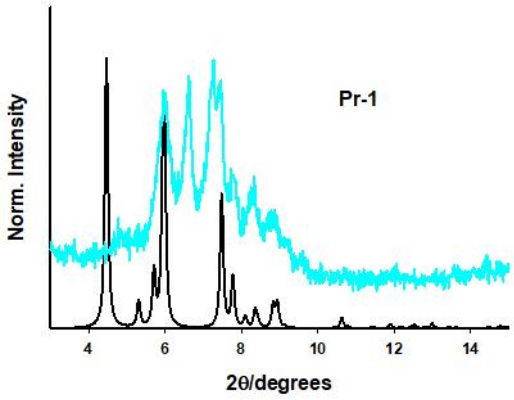
Pr-1
Norm. Intensity
4
6
8
10
12
14
2θ/degrees

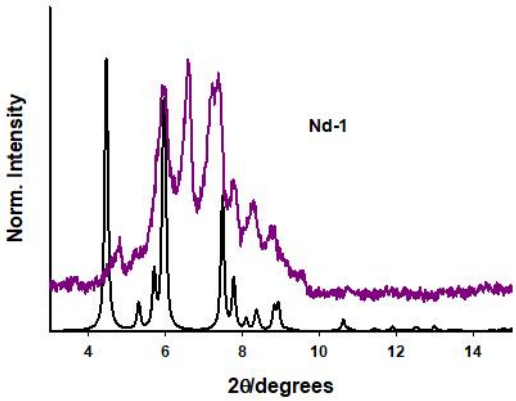
Nd-1
Norm. Intensity
4
6
8
10
12
14
2θ/degrees

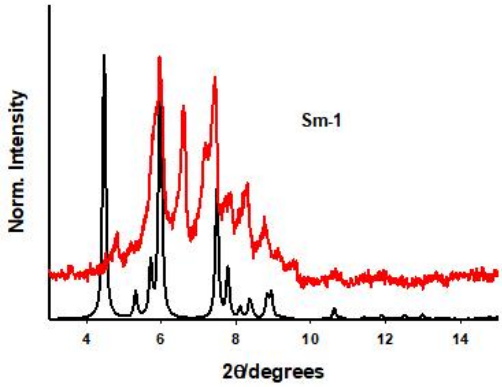
Sm-1
Norm. Intensity
4
6
8
10
12
14
2θ/degrees

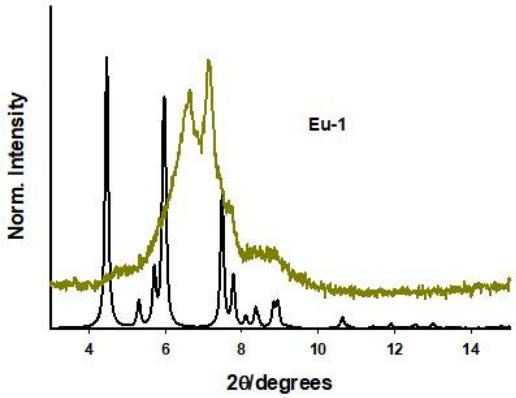
Eu-1
Norm. Intensity
4
6
8
10
12
14
2θ/degrees

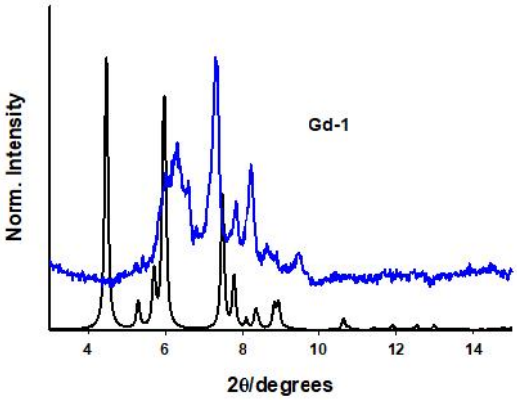
Gd-1
Norm. Intensity
4
6
8
10
12
14
2θ/degrees

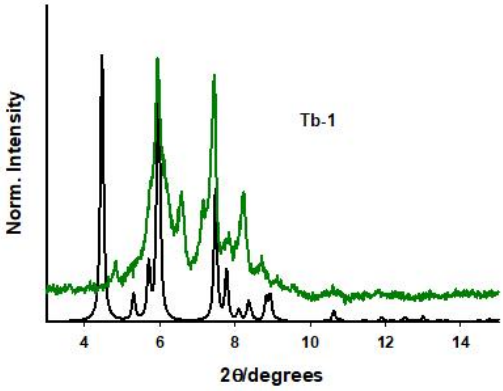
Tb-1
Norm. Intensity
4
6
8
10
12
14
2θ/degrees

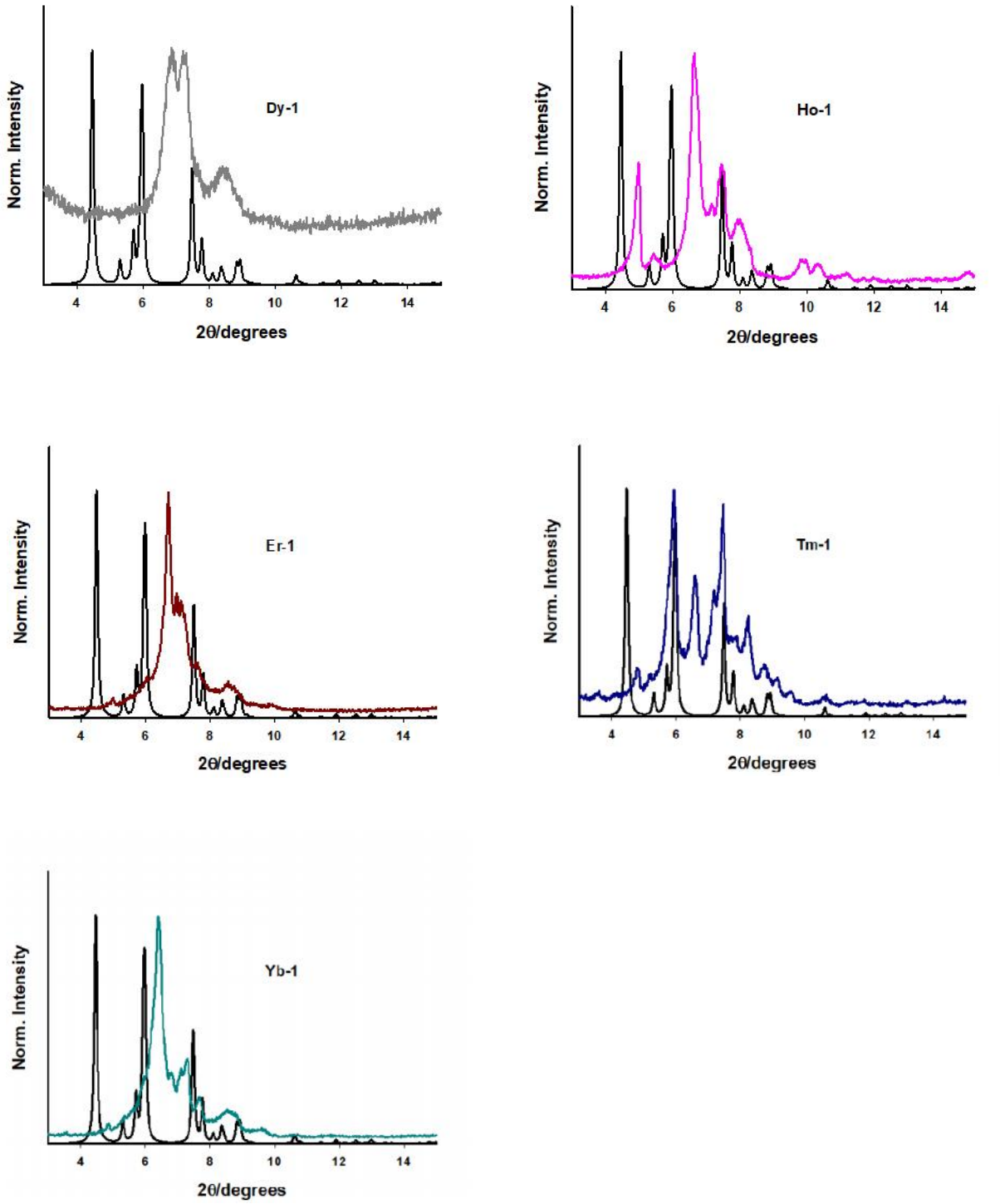

Figure S2b. Powder X-ray diffraction of **Ln-1** metallacryptates compared to a simulated pattern from the **Tb-1** single crystal x-ray data. There is significant deviation due to lattice solvent loss, giving altered reflections and less crystallinity.

ESI-MS

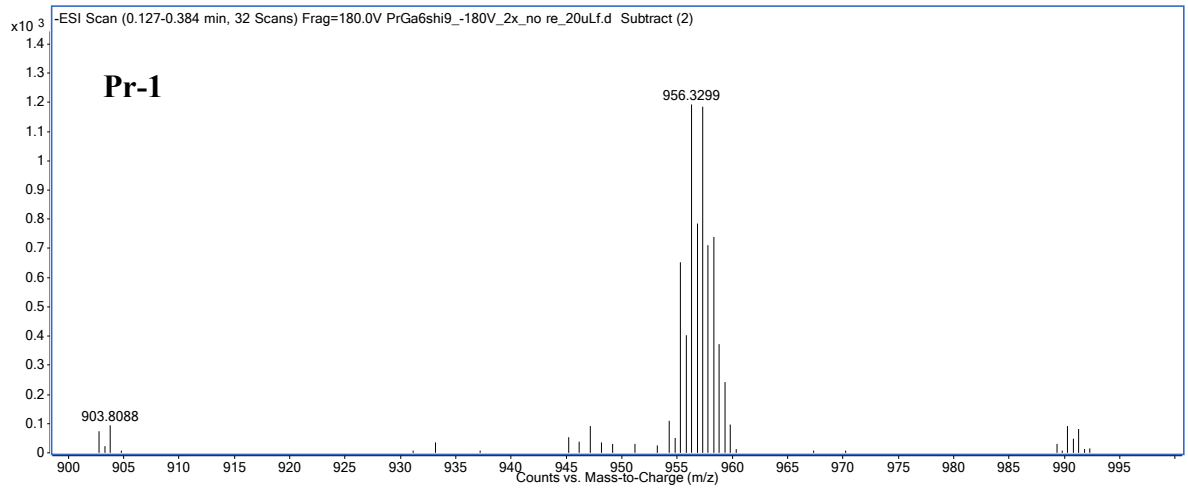
-ESI Scan (0.127-0.384 min, 32 Scans) Frag=180.0V PrGa6shi9_-180V_2x_no re_20uLf.d Subtract (2)
x10 3
Pr-1
956.3299
903.8088
Counts vs. Mass-to-Charge (m/z)

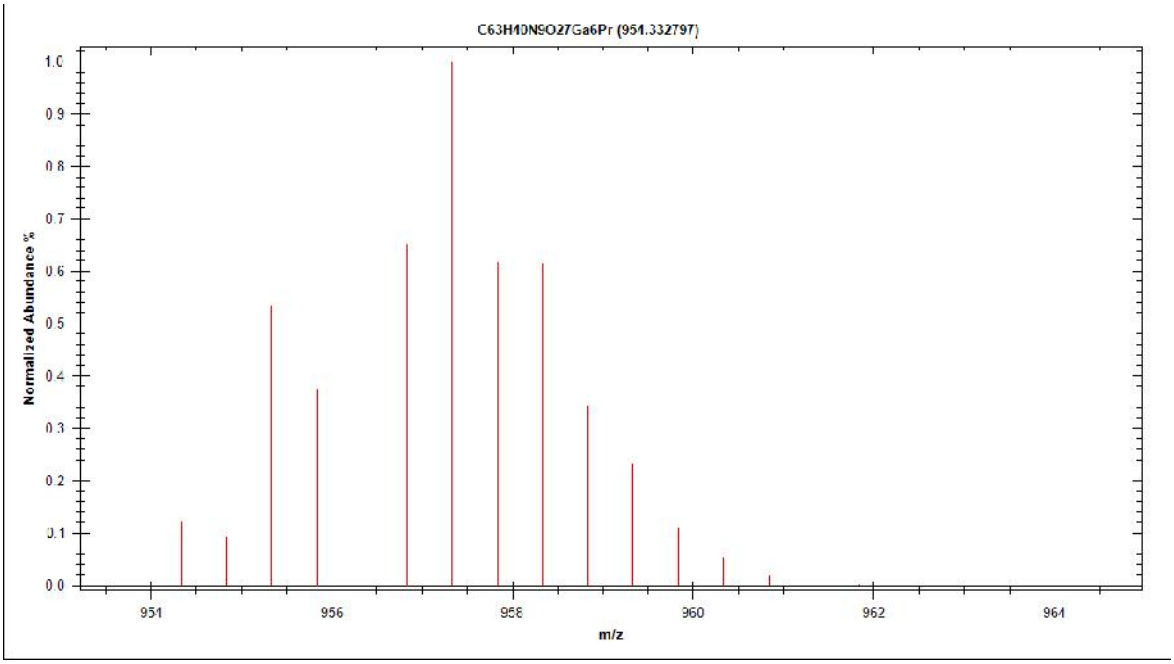
C63H10N9O27Ga6Pr (951.332797)
Normalized Abundance %
m/z

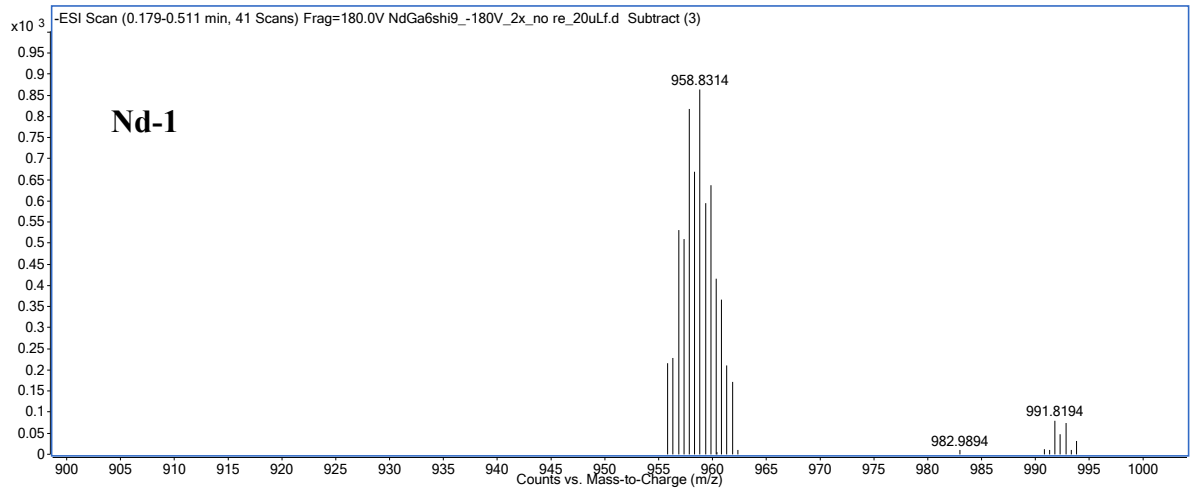
-ESI Scan (0.179-0.511 min, 41 Scans) Frag=180.0V NdGa6shi9_-180V_2x_no re_20uLf.d Subtract (3)
x10 3
Nd-1
958.8314
991.8194
982.9894
Counts vs. Mass-to-Charge (m/z)

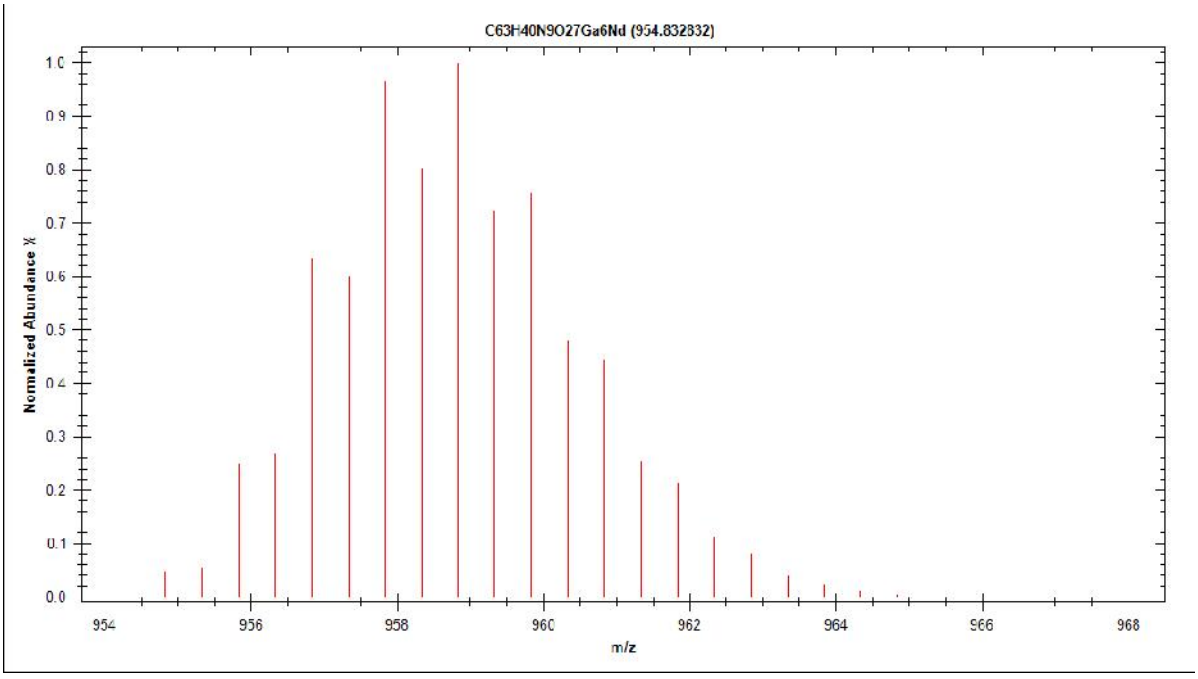
C63H40N9O27Ga6Nd (954.832832)
Normalized Abundance %
m/z

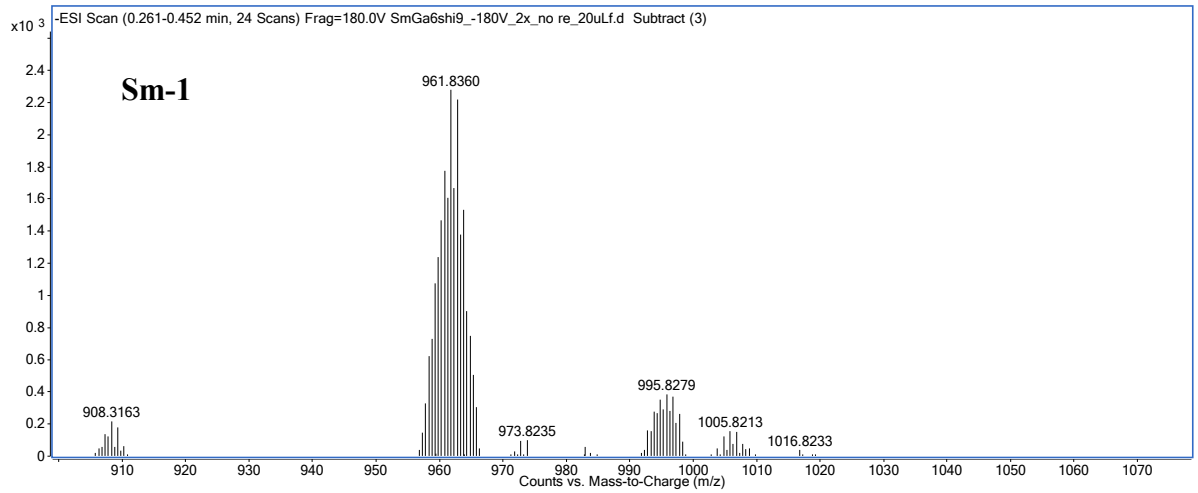
-ESI Scan (0.261-0.452 min, 24 Scans) Frag=180.0V SmGa6shi9_-180V_2x_no re_20uLf.d Subtract (3)
x10 3
Sm-1
961.8360
908.3163
973.8235
995.8279
1005.8213
1016.8233
Counts vs. Mass-to-Charge (m/z)

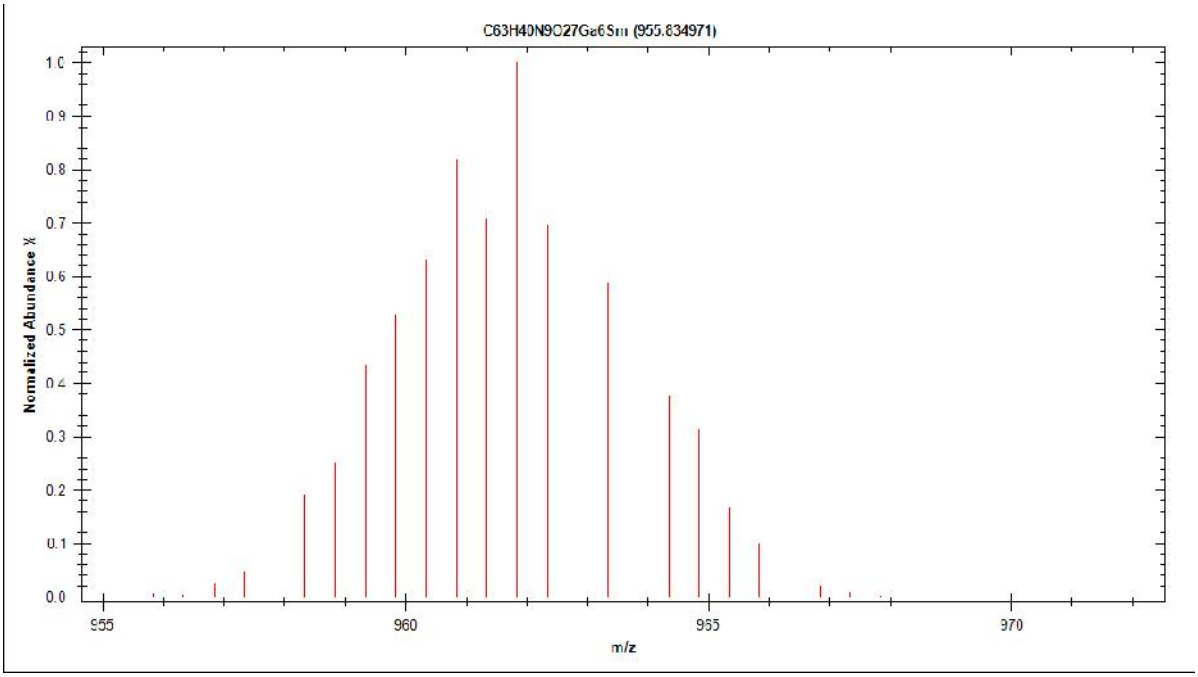
Normalized Abundance %
m/z

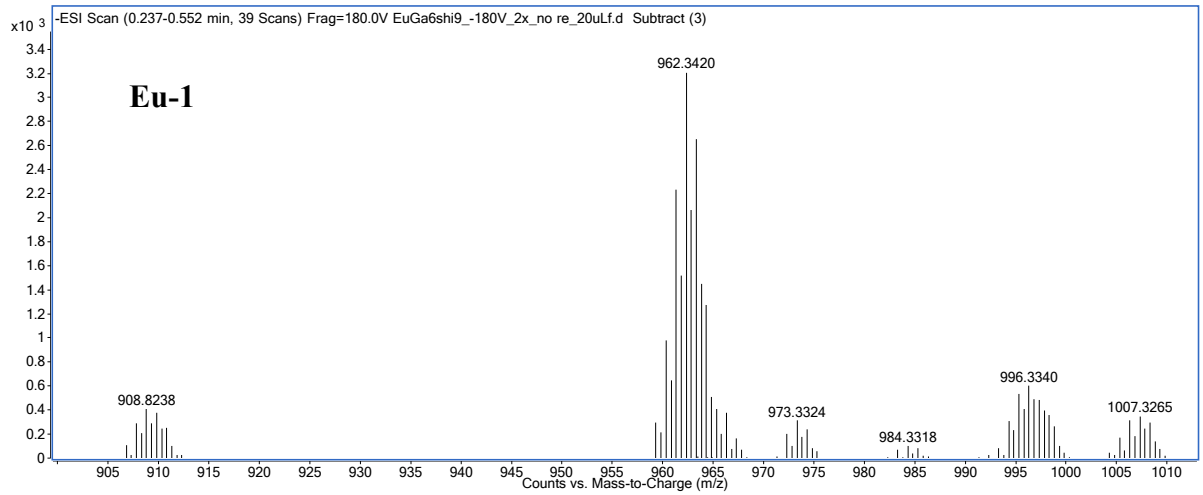
-ESI Scan (0.237-0.552 min, 39 Scans) Frag=180.0V EuGa6shi9_-180V_2x_no re_20uLf.d Subtract (3)
x10 3
Eu-1
962.3420
908.8238
973.3324
984.3318
996.3340
1007.3265
Counts vs. Mass-to-Charge (m/z)

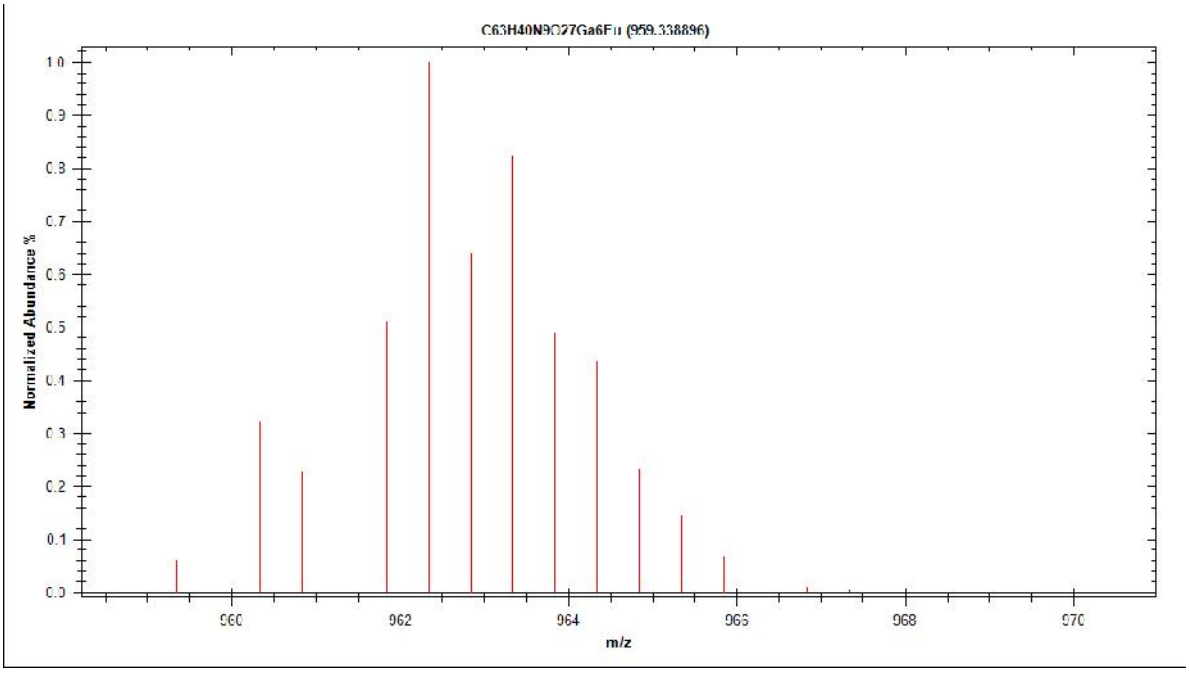
Normalized Abundance %
m/z

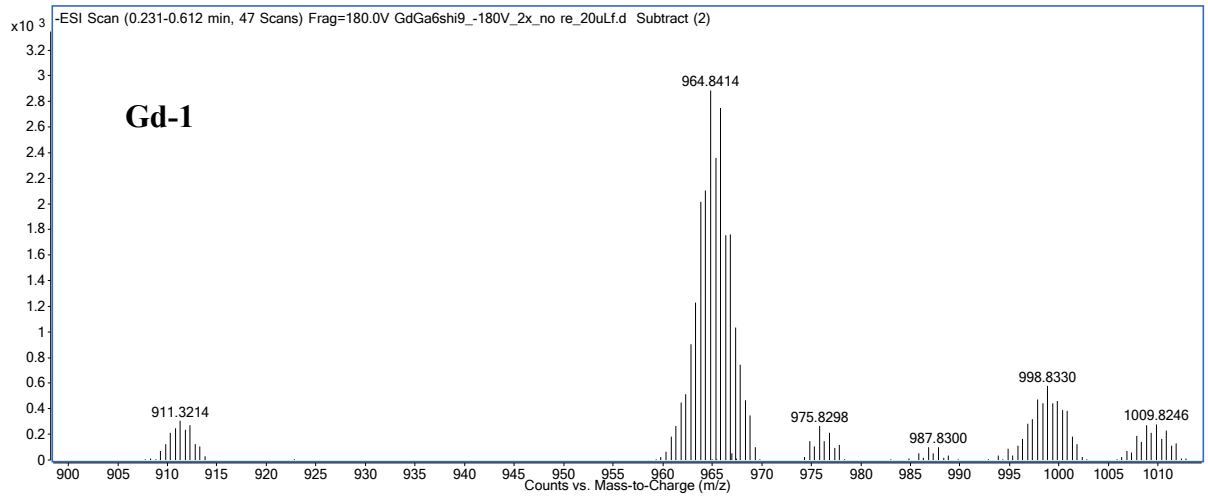
-ESI Scan (0.231-0.612 min, 47 Scans) Frag=180.0V GdGa6shi9_-180V_2x_no re_20uLf.d Subtract (2)
x10 3
Gd-1
964.8414
911.3214
975.8298
987.8300
998.8330
1009.8246
Counts vs. Mass-to-Charge (m/z)

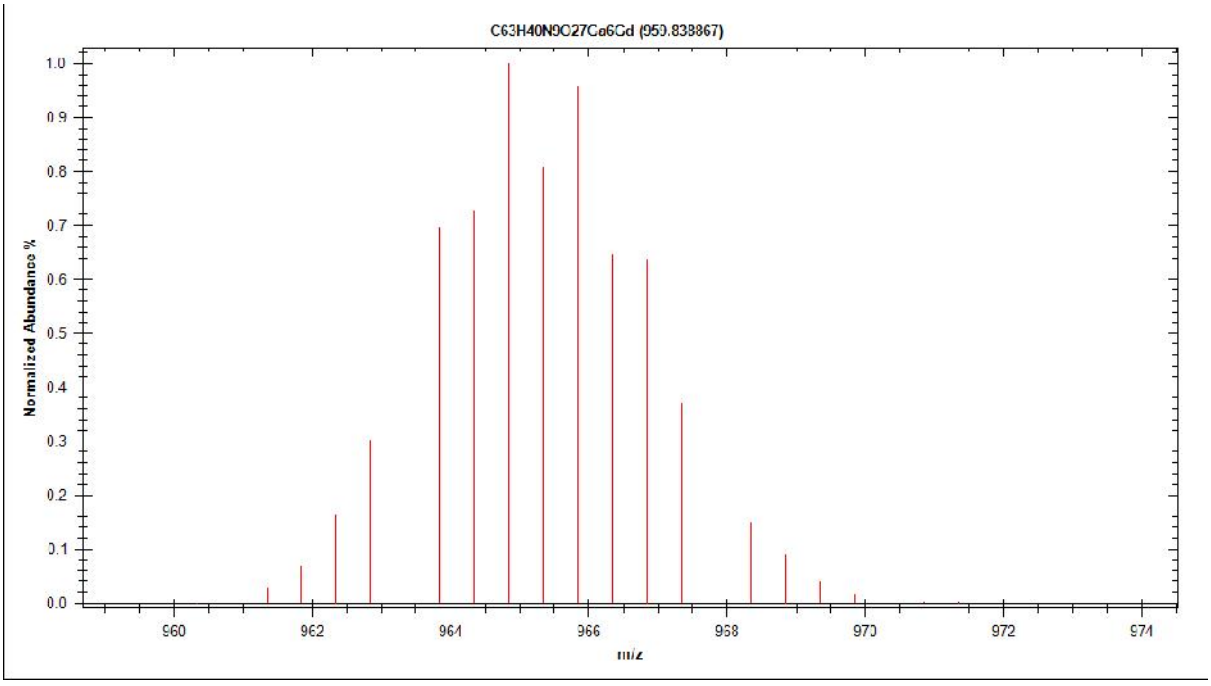
C63H40N9O27Ga6Gd (959.838867)
Normalized Abundance %
m/z

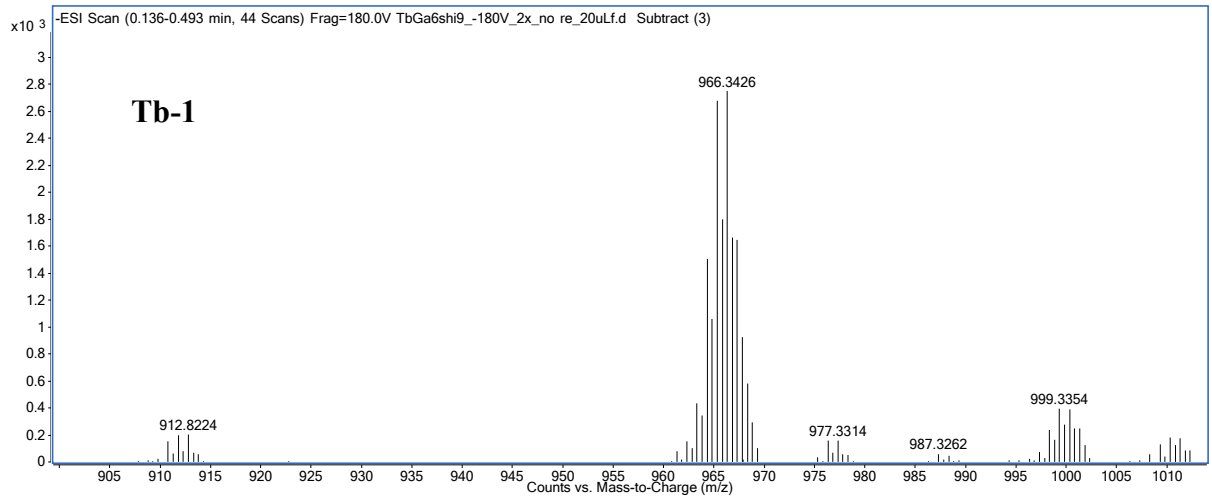
-ESI Scan (0.136-0.493 min, 44 Scans) Frag=180.0V TbGa6shi9_-180V_2x_no re_20uLf.d Subtract (3)
x10 3
Tb-1
966.3426
912.8224
977.3314
987.3262
999.3354
Counts vs. Mass-to-Charge (m/z)

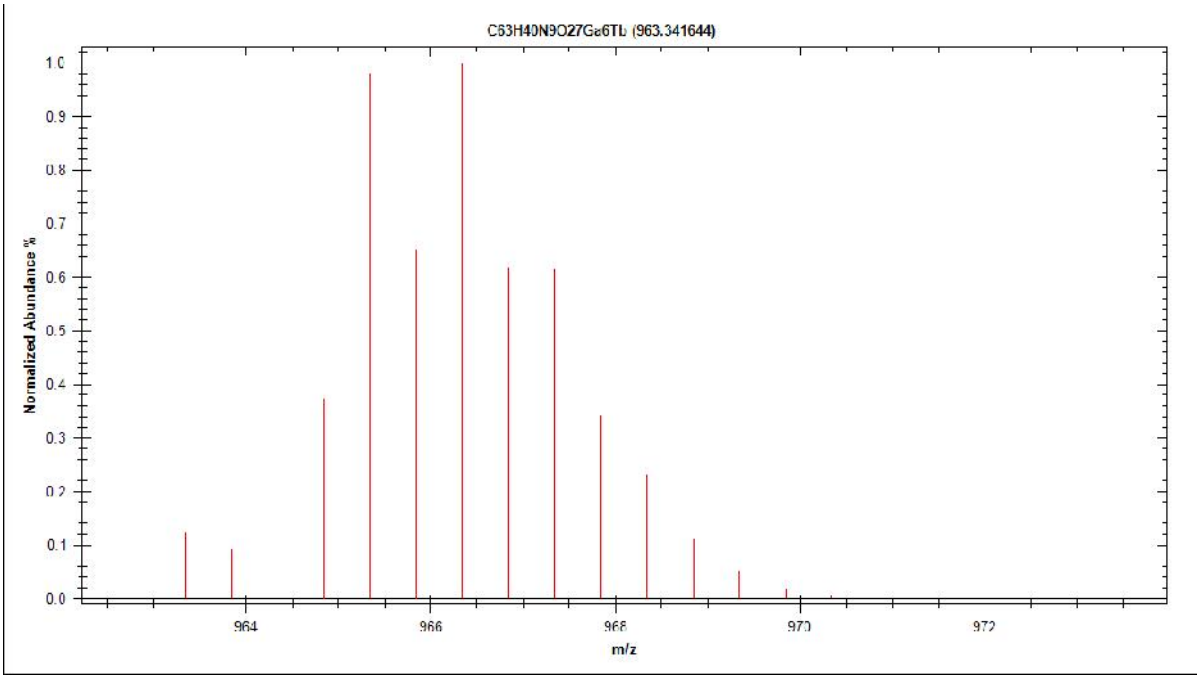
Normalized Abundance %
m/z

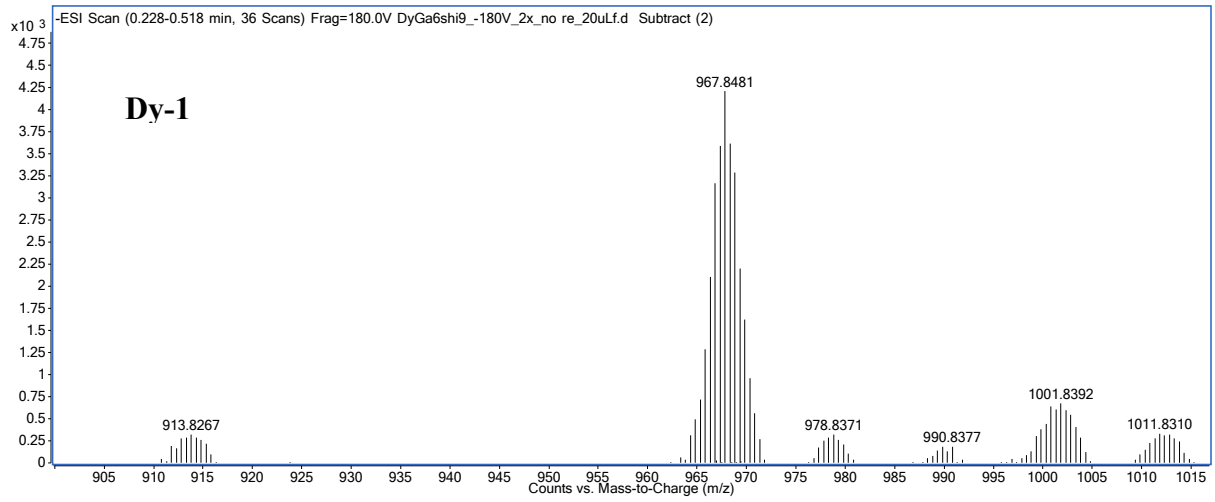
-ESI Scan (0.228-0.518 min, 36 Scans) Frag=180.0V DyGa6shi9_-180V_2x_no re_20uLf.d Subtract (2)
x10 3
Dy-1
967.8481
913.8267
978.8371
990.8377
1001.8392
1011.8310
Counts vs. Mass-to-Charge (m/z)

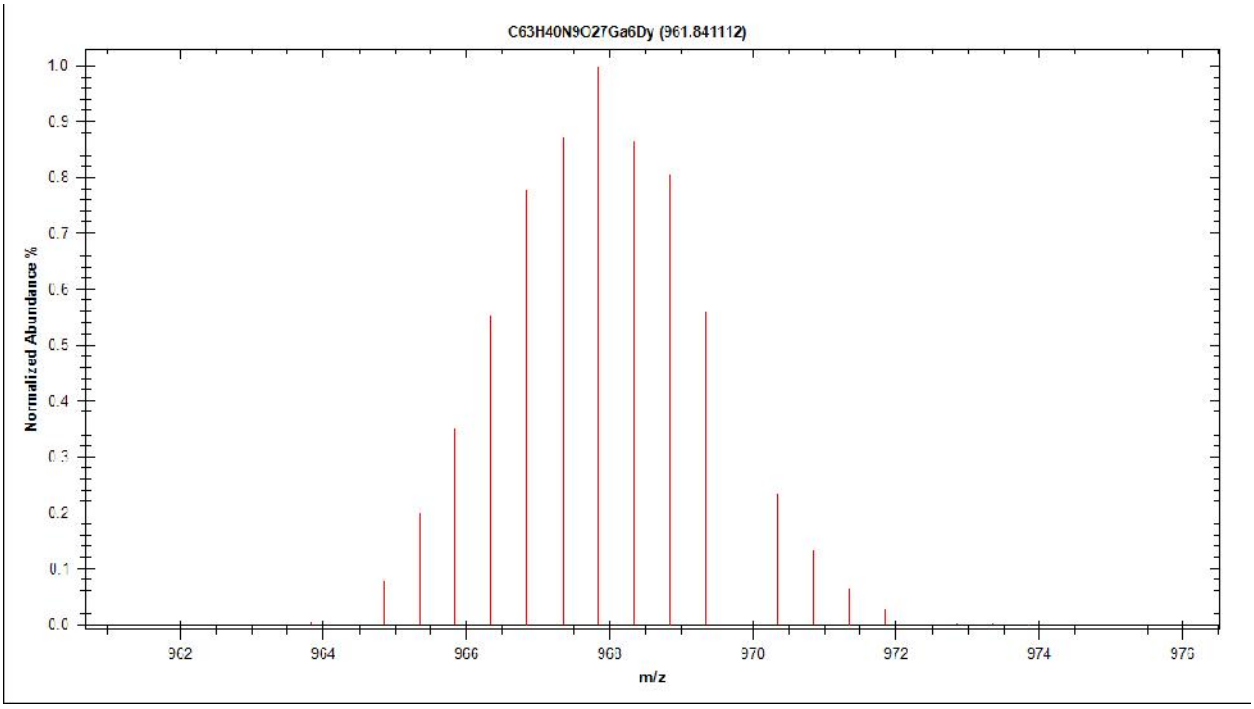
C63H40N9O27Ga6Dy (961.841112)
Normalized Abundance %
m/z

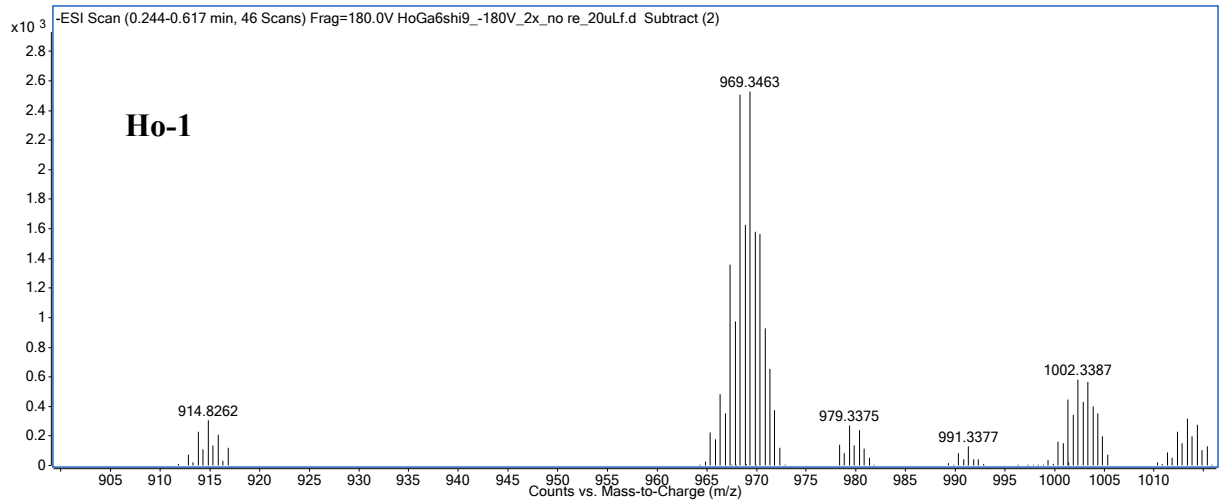
-ESI Scan (0.244-0.617 min, 46 Scans) Frag=180.0V HoGa6shi9_-180V_2x_no re_20uLf.d Subtract (2)
x10 3
Ho-1
969.3463
914.8262
979.3375
991.3377
1002.3387
Counts vs. Mass-to-Charge (m/z)

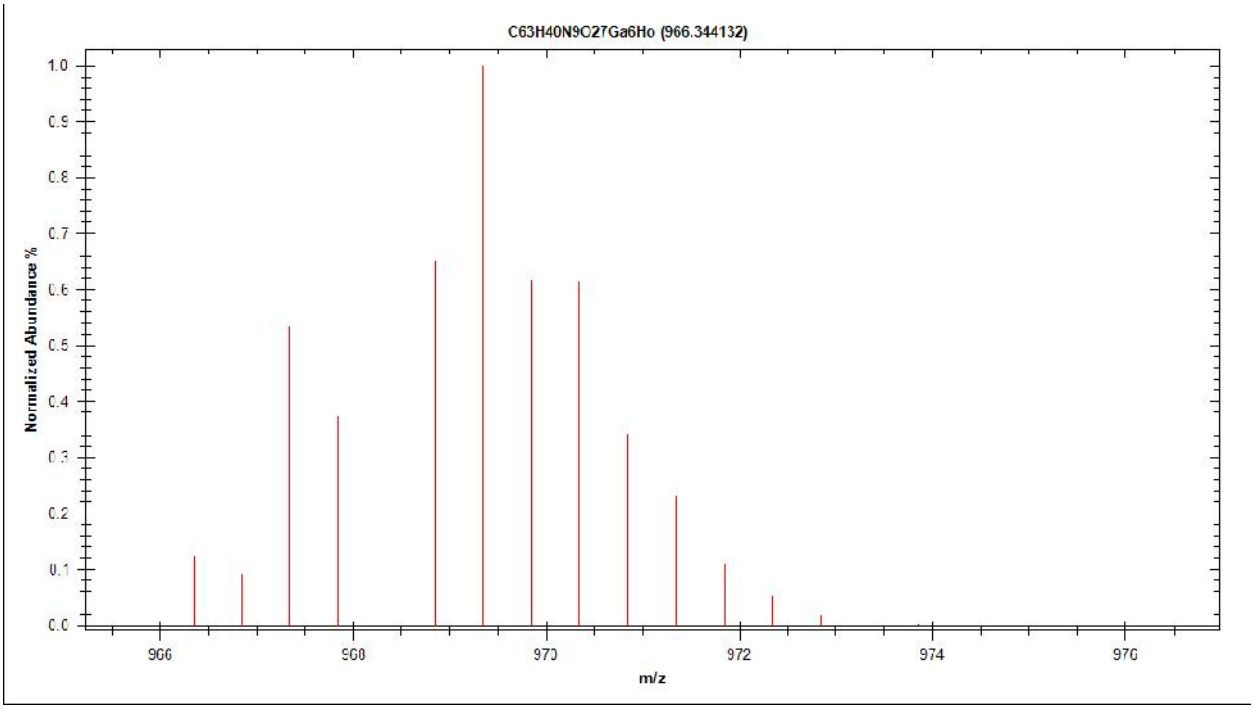
C63H40N9C27Ga6Ho (966.344132)
Normalized Abundance %
m/z

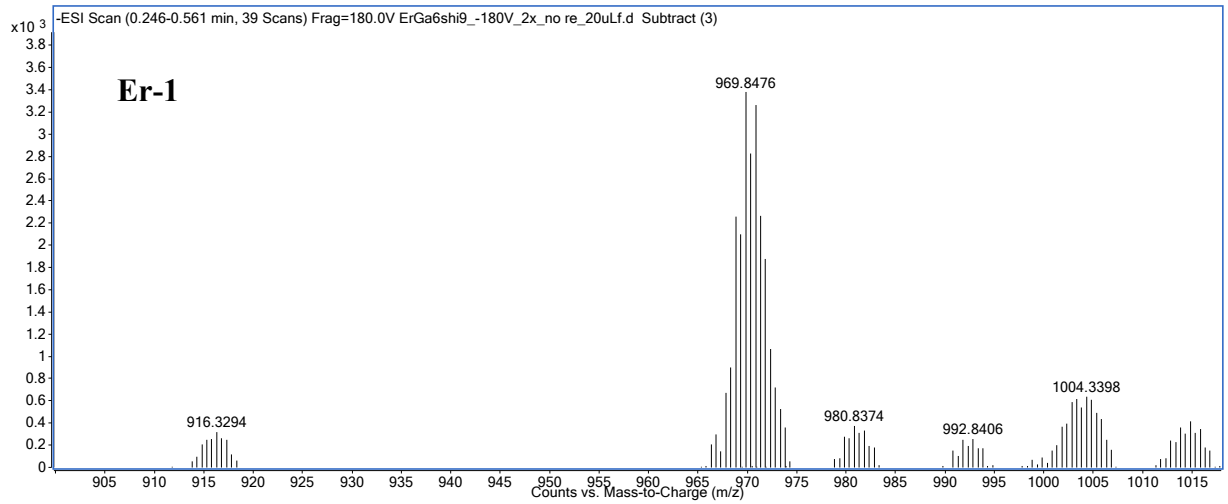
-ESI Scan (0.246-0.561 min, 39 Scans) Frag=180.0V ErGa6shi9_-180V_2x_no re_20uLf.d Subtract (3)
x10 3
Er-1
969.8476
916.3294
980.8374
992.8406
1004.3398
Counts vs. Mass-to-Charge (m/z)

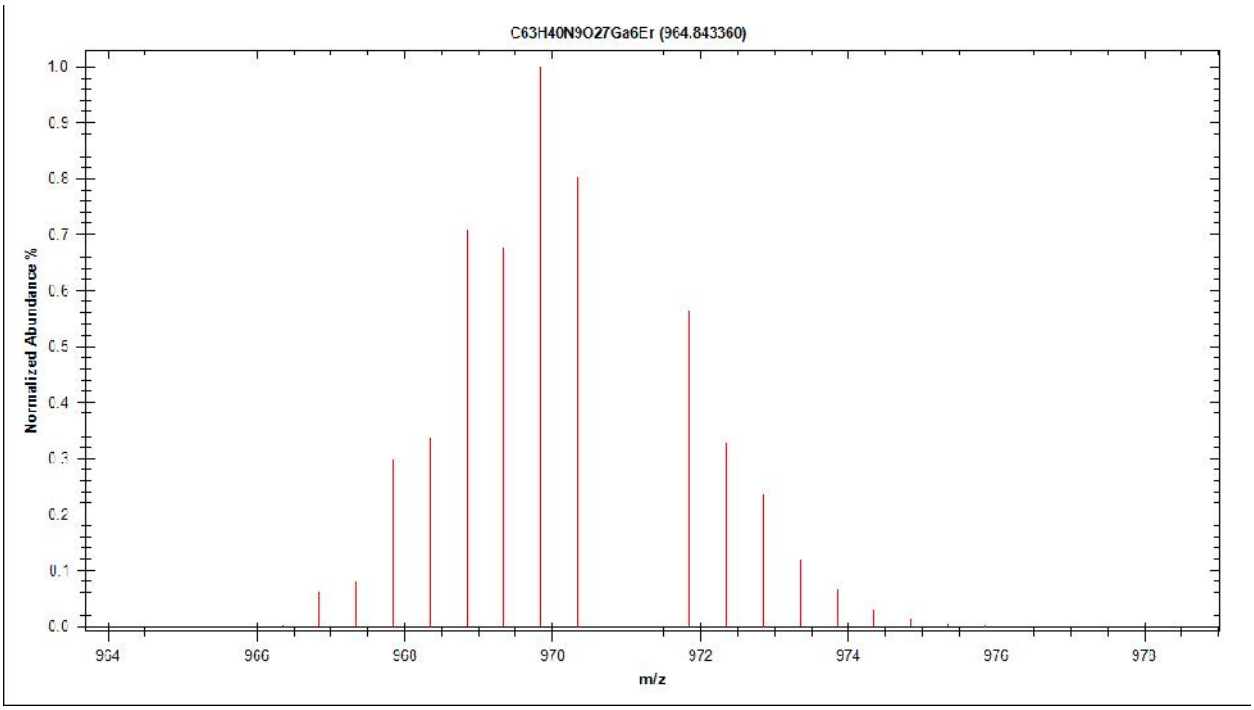
C63H40N9O27Ga6Er (964.843360)
Normalized Abundance %
m/z

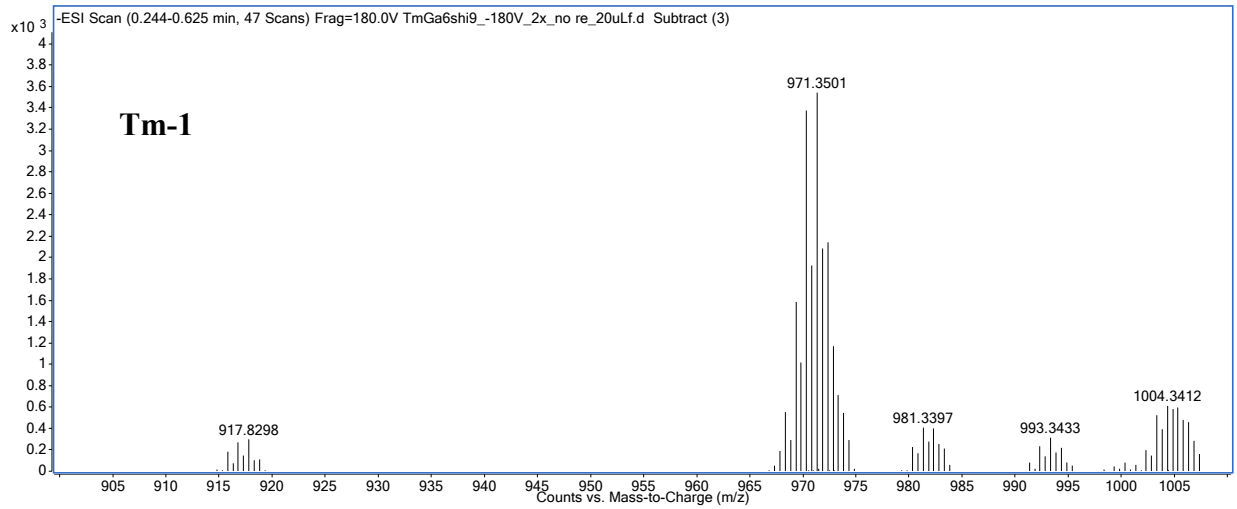
-ESI Scan (0.244-0.625 min, 47 Scans) Frag=180.0V TmGa6shi9_-180V_2x_no re_20uLf.d Subtract (3)
x10 3
Tm-1
971.3501
917.8298
981.3397
993.3433
1004.3412
Counts vs. Mass-to-Charge (m/z)

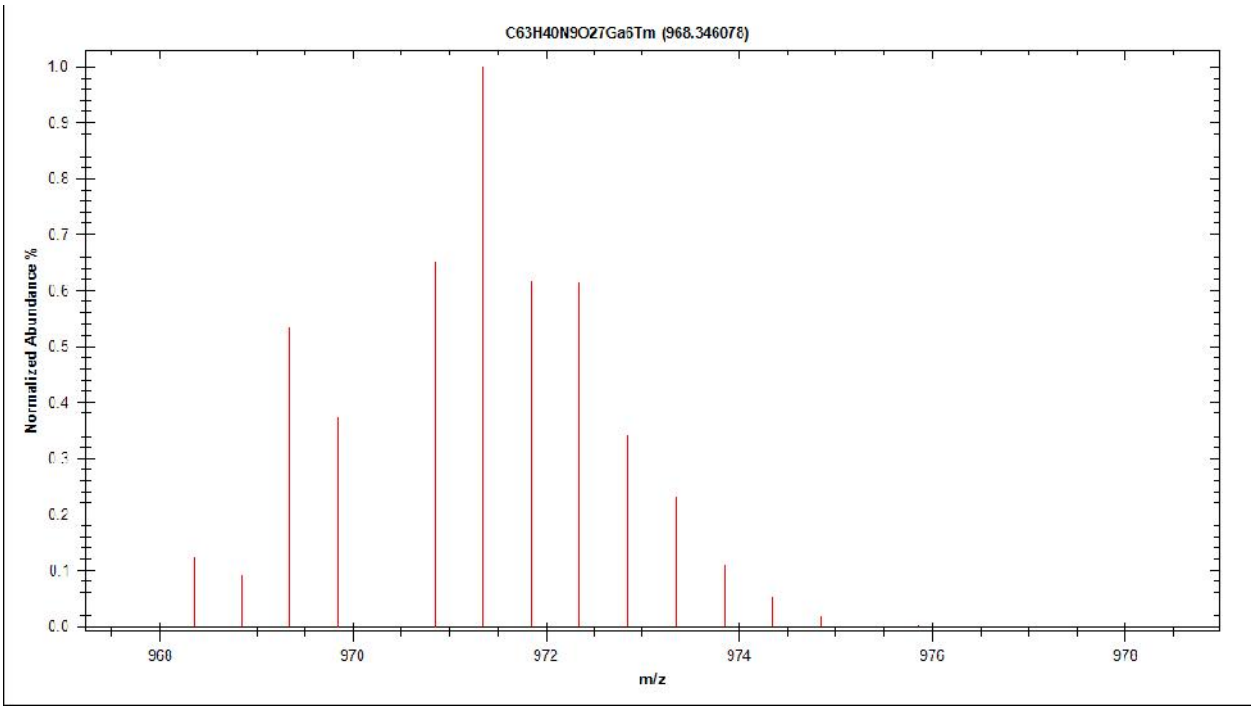
C63H40N9O27Ga5Tm (968.346078)
Normalized Abundance %
m/z

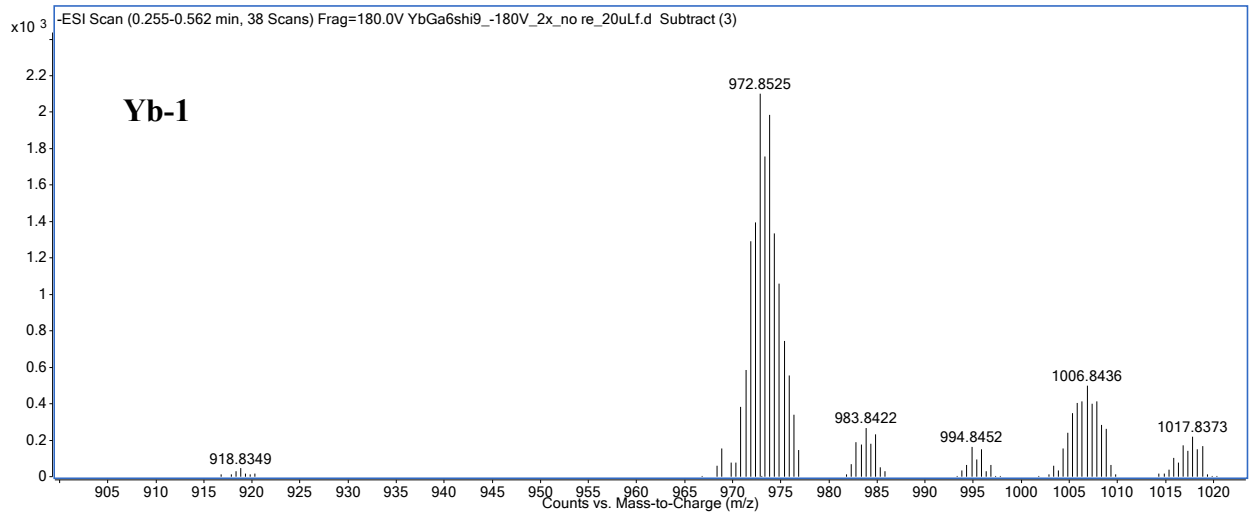
-ESI Scan (0.255-0.562 min, 38 Scans) Frag=180.0V YbGa6shi9_-180V_2x_no re_20uLf.d Subtract (3)
x10 3
Yb-1
972.8525
983.8422
994.8452
1006.8436
1017.8373
918.8349
Counts vs. Mass-to-Charge (m/z)

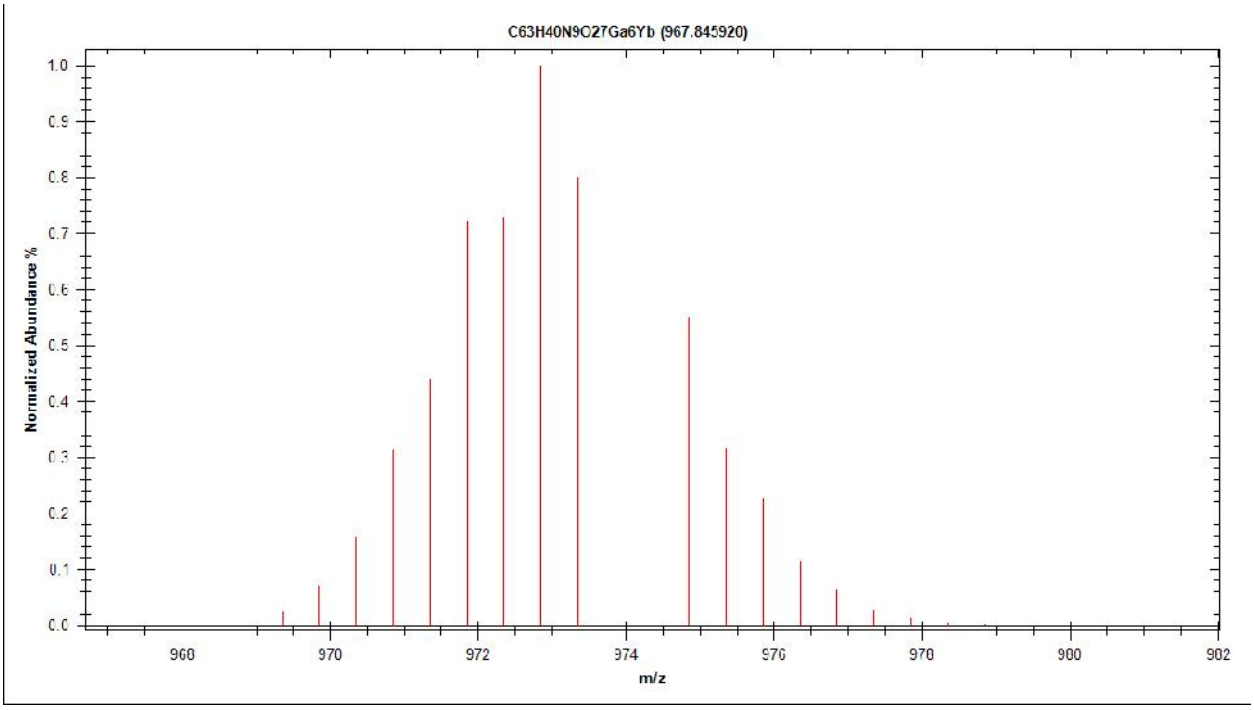
C63H40N9C27Ga6Yb (967.845920)
Normalized Abundance %
m/z

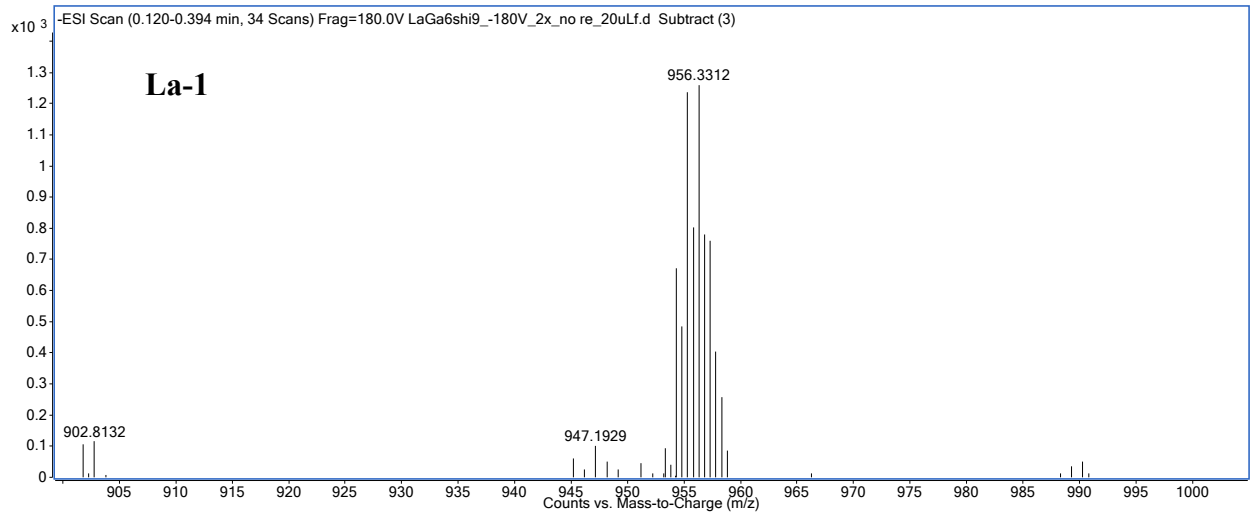
-ESI Scan (0.120-0.394 min, 34 Scans) Frag=180.0V LaGa6shi9_-180V_2x_no re_20uLf.d Subtract (3)
x10 3
La-1
956.3312
902.8132
947.1929
Counts vs. Mass-to-Charge (m/z)

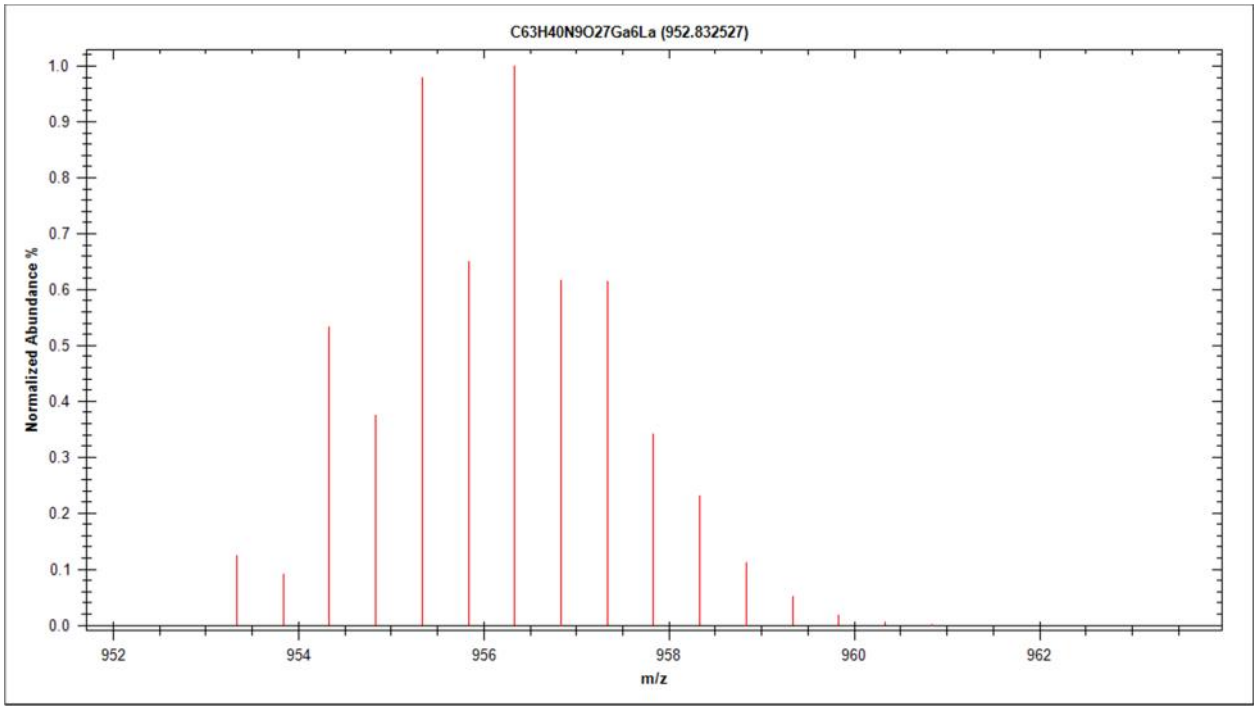
C63H40N9O27Ga6La (952.832527)
Normalized Abundance %
m/z

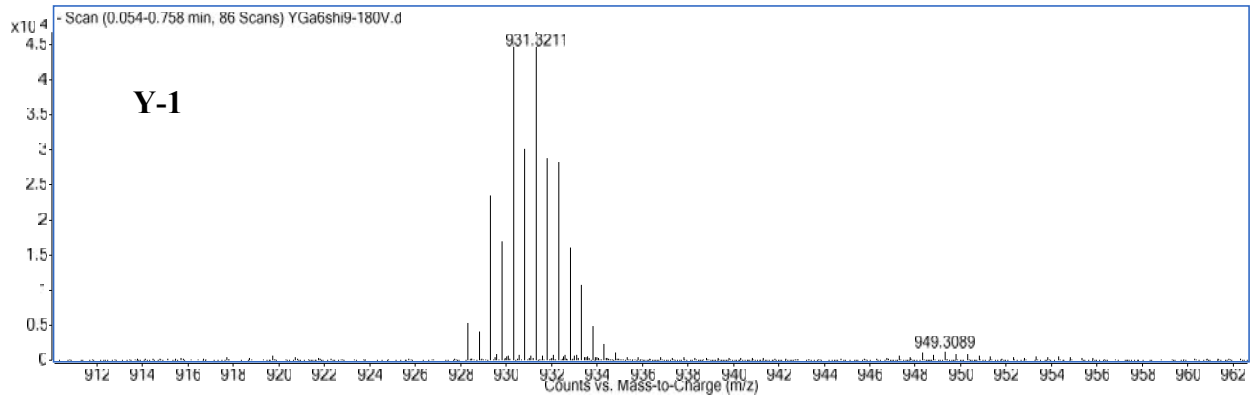
- Scan (0.054-0.758 min, 86 Scans) YGa6shi9-180V.d
x10 4
Y-1
931.3211
949.3089
Counts vs. Mass-to-Charge (m/z)

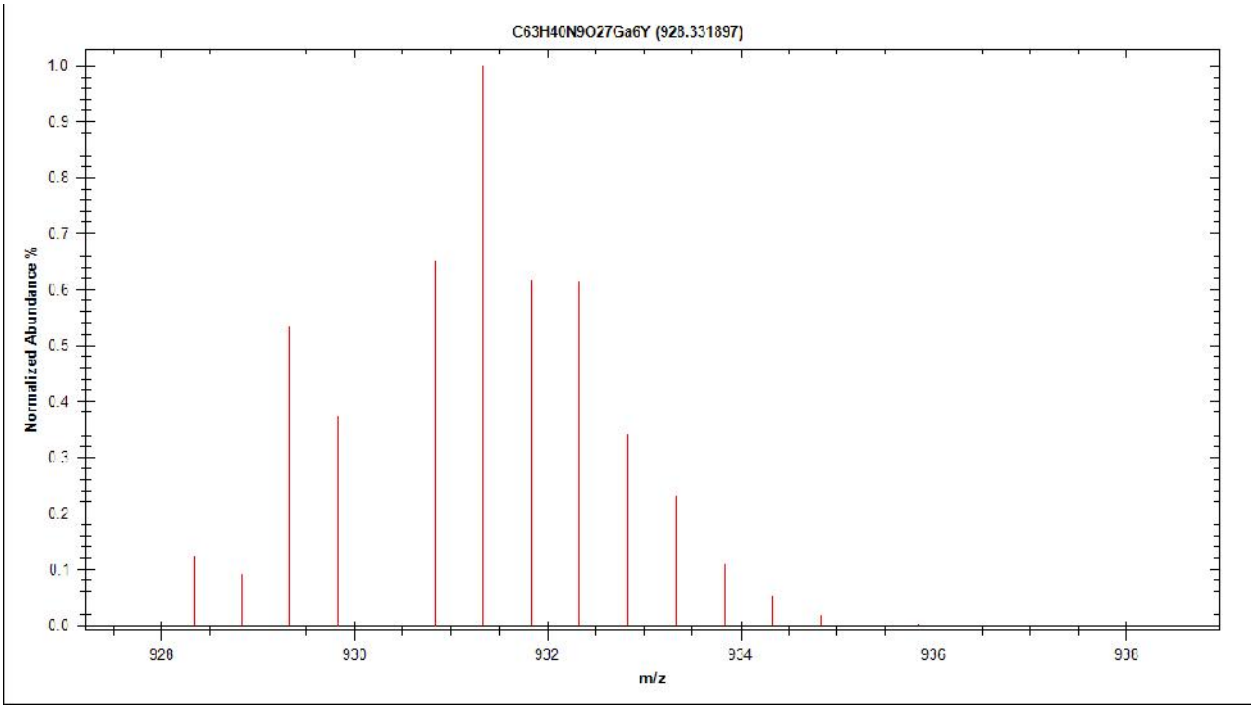
C63H40N9O27Ga6Y (928.331897)
Normalized Abundance %
m/z

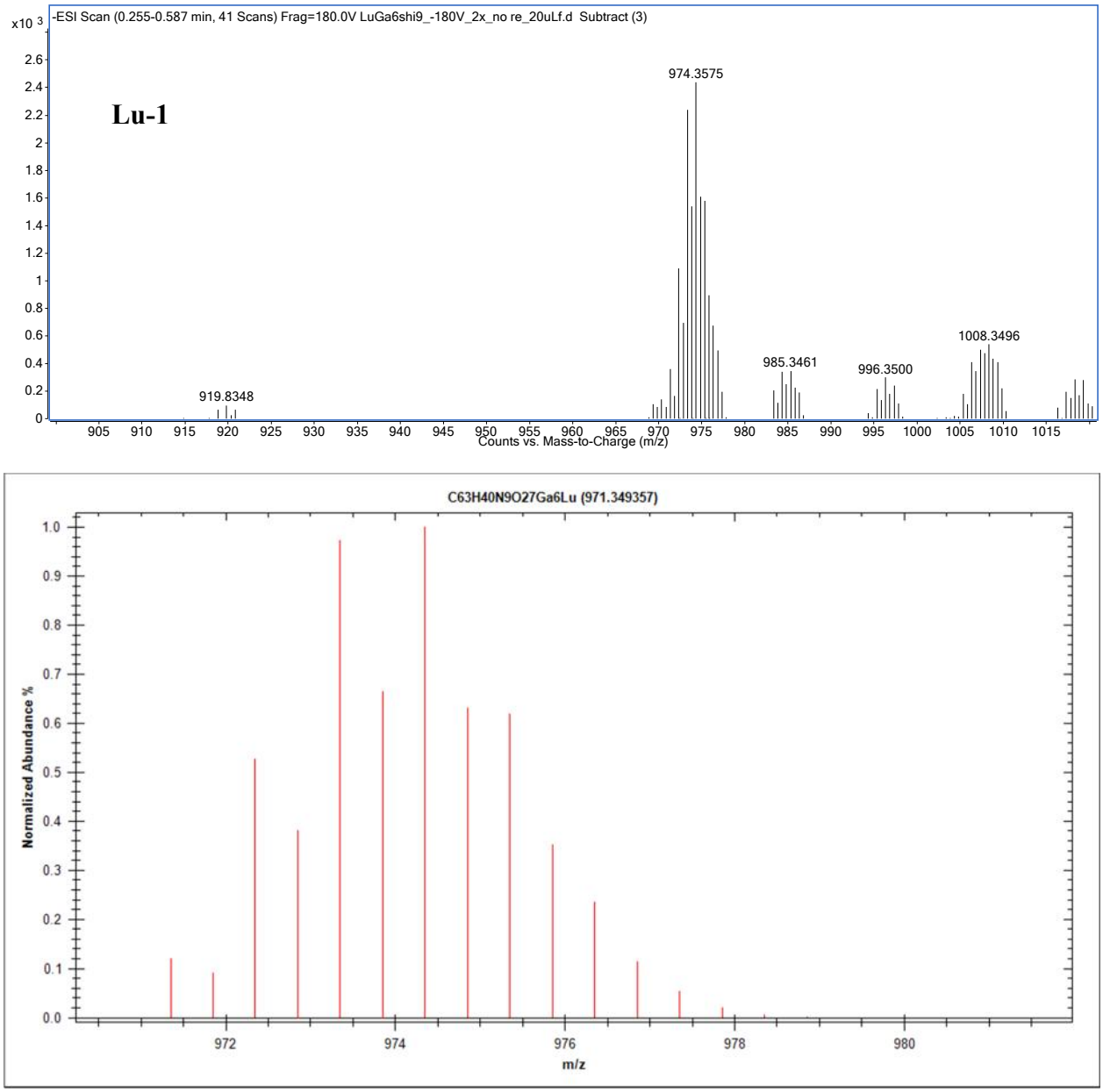

Figure S3. ESI-QTOF mass-spectra of **Ln-1** complexes and simulated spectra of each analog. Spectra collected in negative ion mode with fragmentation voltage of 180 V. Background spectra were subtracted three times.

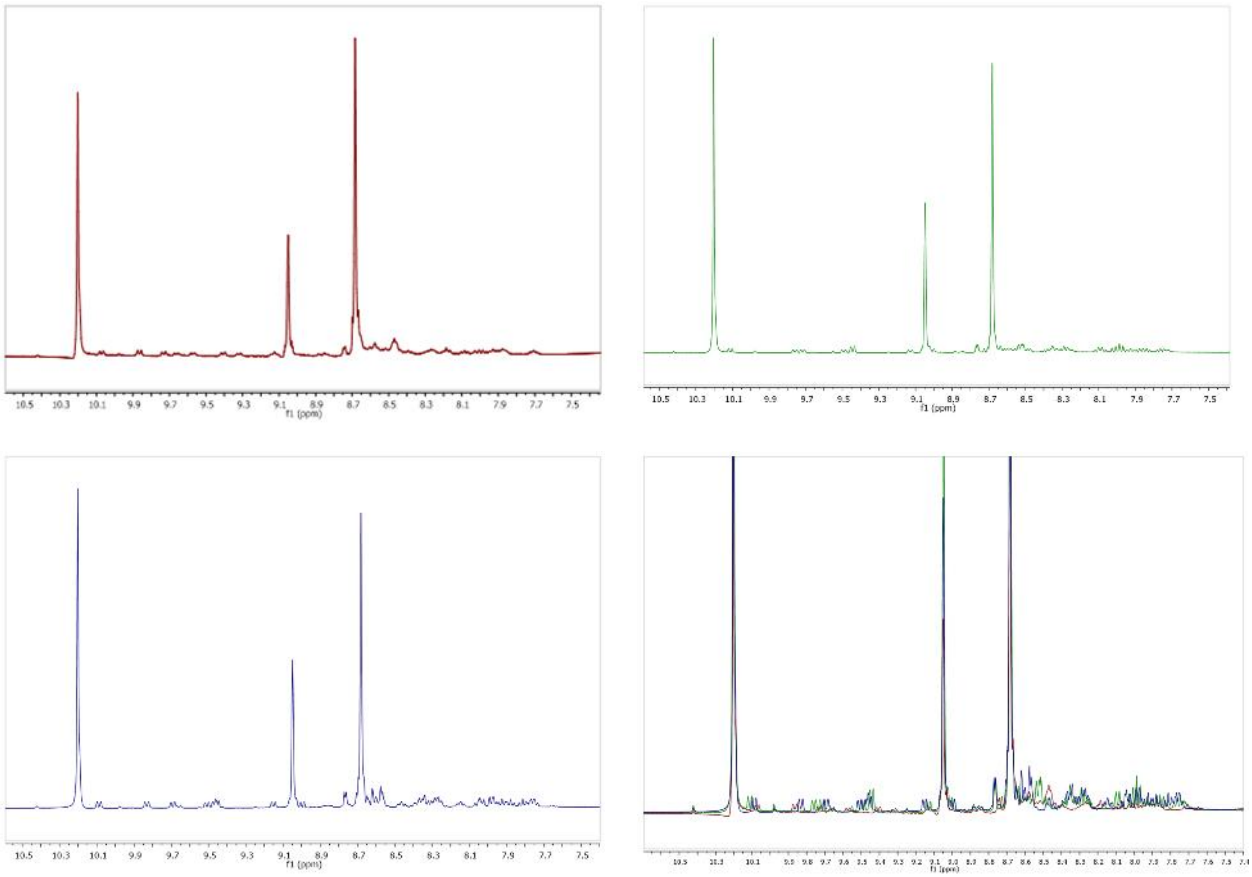

Figure S4. ^{1}H-NMR of a) **La-1**, b) **Y-1**, c) **Lu-1** and d) overlay of all three in d_5-pyridine at RT.

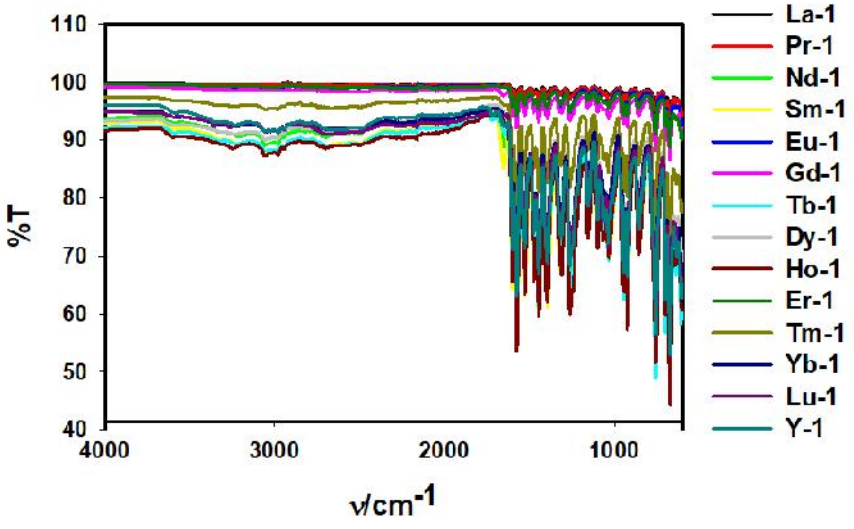

Figure S5. FT-IR of **Ln-1** complexes.

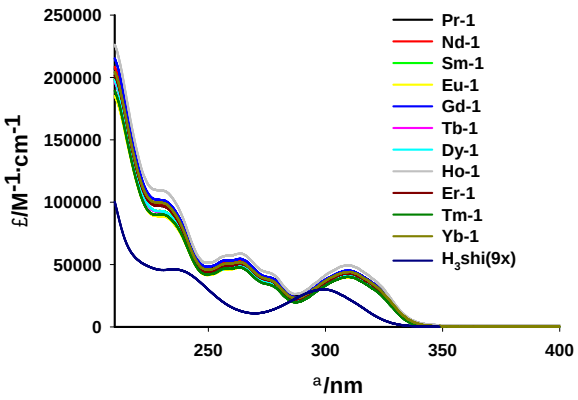

Figure S6. UV-vis absorption spectra of 1-10 μM **Ln-1** metallacryptates and H_3shi ligand (multiplied by 9 to match the number of ligands present in the complex) in methanol solution at room temperature.

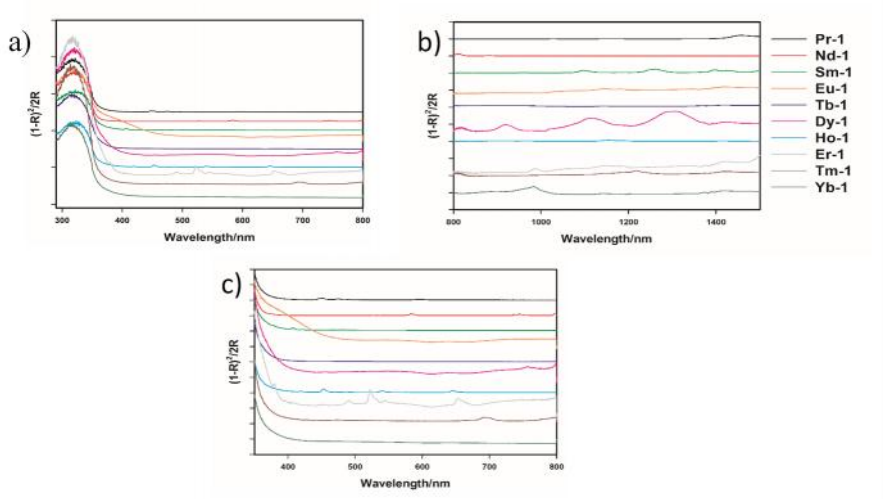

Figure S7. Solid state diffuse reflectance spectra of **Ln-1** complexes; a) UV-vis region; b) near-infrared region; c) zoom in on f-f transitions in the visible. Trace colors are as follows: black = Pr, red = Nd, green = Sm, orange = Eu, blue = Tb, pink = Dy, aqua = Ho, gray = Ho, brown = Tm, dark green = Yb.

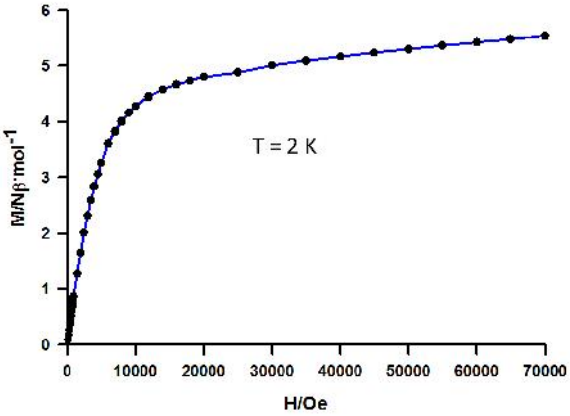

Figure S8. Isothermal magnetization of **Dy-1** at 2K. The blue line is a guide for the eye.

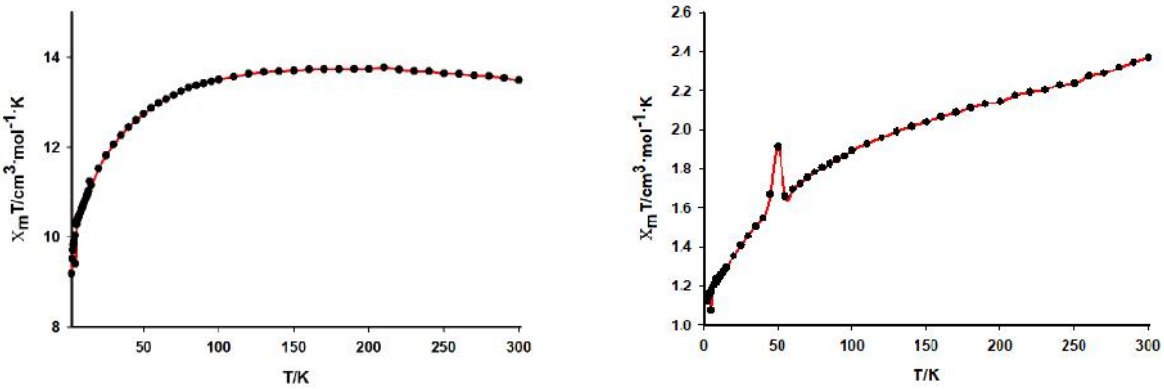

Figure S9. DC magnetic susceptibility of **Dy-1** (top left), **Nd-1** (top right), and **Yb-1** (bottom) in a 2000 Oe applied field. Red lines are a guide for the eye.

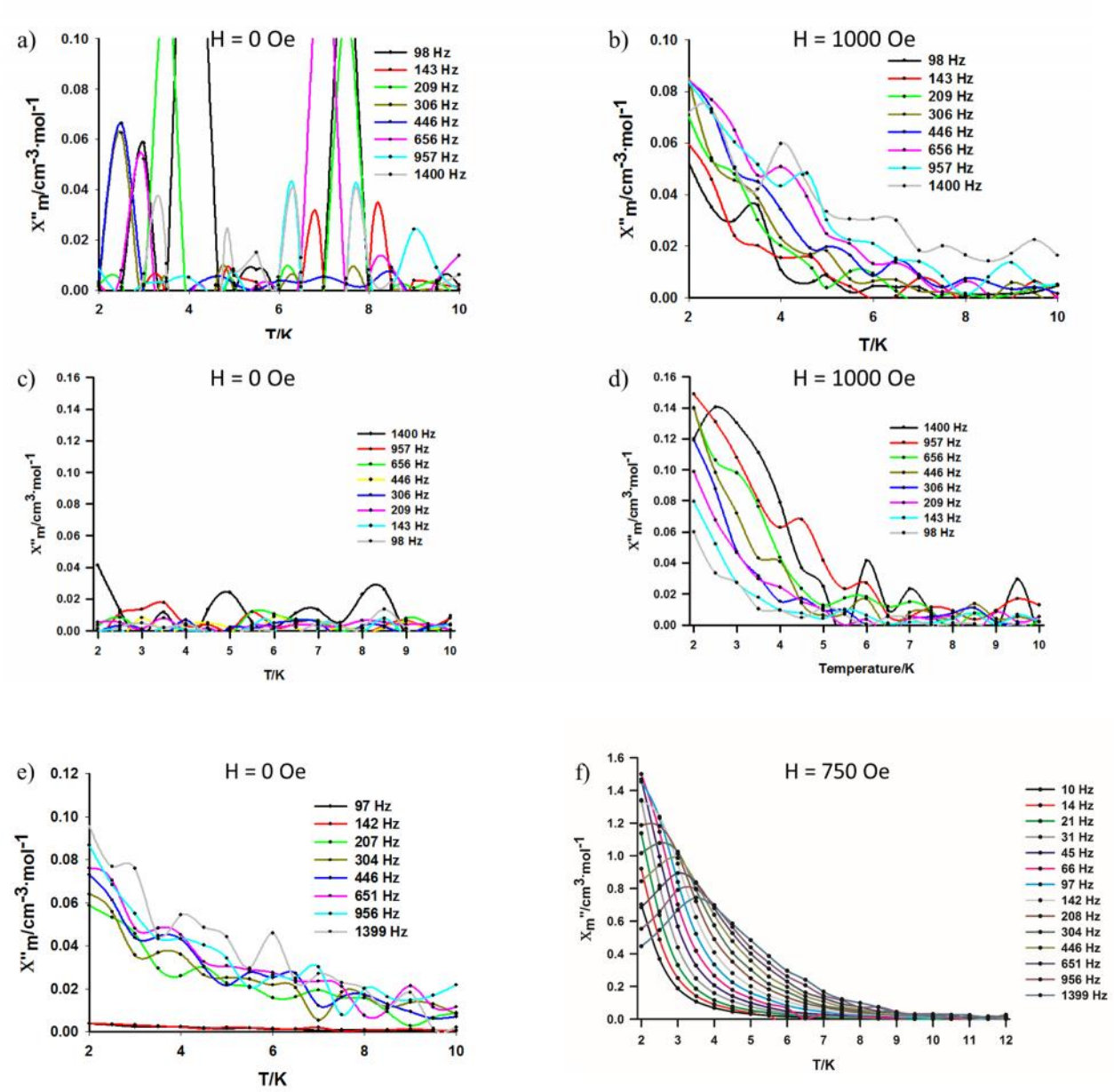

Figure S11. AC out of phase susceptibility measurements of **Ln-1** using a 3 Oe drive field. a) **Nd-1** with zero applied field and b) applied field of 1000 Oe; c) **Yb-1** with zero applied field and d) applied field of 1000 Oe; e) **Dy-1** with zero applied field and f) applied field of 750 Oe.

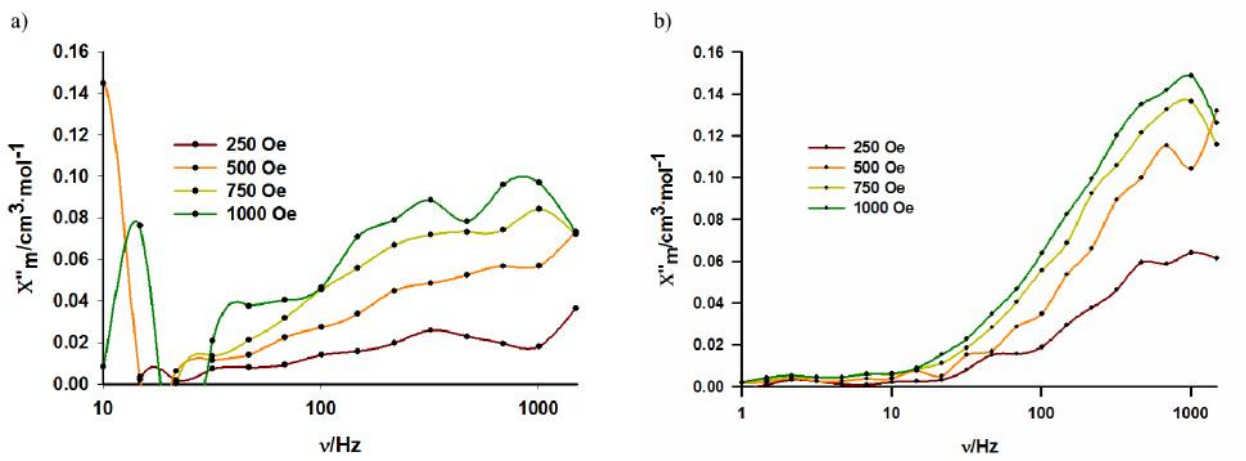

Figure S12. Variable frequency AC out of phase behavior of a) **Nd-1** and b) **Yb-1** in various applied DC fields at 2K.

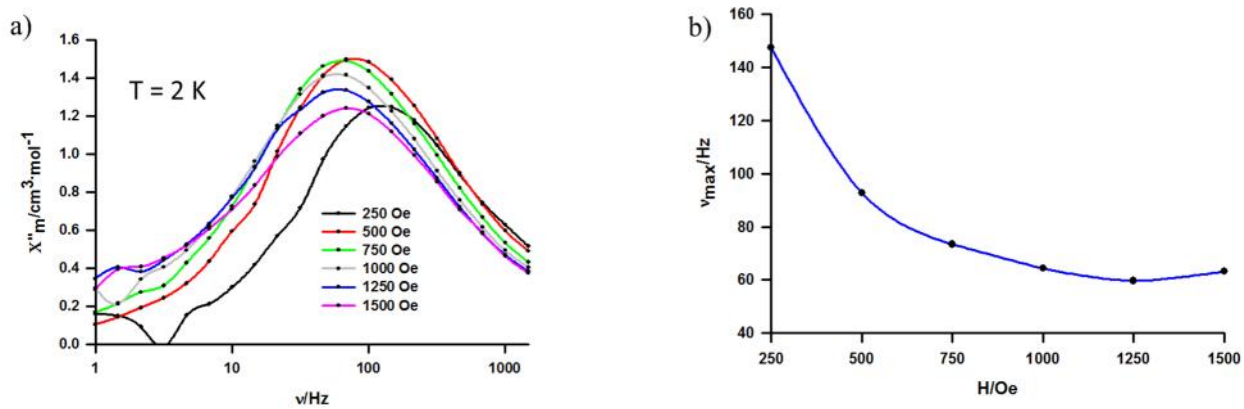

Figure S13. a) Variable frequency AC out of phase behavior of **Dy-1** in various applied fields at 2 K; b) plot of ν_{max} minimization as a function of applied field H. ν_{max} was determined from fitting a logarithmic peak function $\chi m'' = a \cdot e\text{^}((-0.5 \cdot (ln(\nu/\nu\_max)/2)\text{^}2))$. 750 Oe is chosen since this field showed a low ν_{max} and still had a high χ''_m signal.

Table S1. Comparison of photophysical parameters of Gd^{3+}/Ln^{3+} MCs([Ln[12-MC-4])[a] and metallacryptates **Ln-1** (Ln[3.3.1])

Lanthanide Complex	**ε/$M^{-1}\cdot cm^{-1}$[b]**	**q^{L}_{Ln} /%**	**τ_{obs} / µs**
Sm[12-MC-4]	21910	2.91(8)[c]	148(1)
Sm[3.3.1]	42184	1.70(9)[c]	70(1)
Tb[12-MC-4]	22517	34.7(1)	1080(10)
Tb[3.3.1]	40733	0.189(3)	20.7(5) : 71% 4.54(6) : 29%
Ho[12-MC-4]	23246	$2.0(2)\cdot10^{-3}$	0.029(1)
Ho[3.3.1]	49267	$1.1(2)\cdot10^{-3}$	0.037(1)
Er[12-MC-4]	20133	0.044(1)	6.75(3)
Er[3.3.1]	42879	$7.1(2)\cdot10^{-3}$	0.905(8)
Yb[12-MC-4]	21934	5.88(2)	55.7(3)
Yb[3.3.1]	43975	0.65(3)	7.26(2)

[a] Taken from Ref.[1]

[b] Molar absorption coefficients are given at 310nm for both Ln[12-MC-4] and Ln[3.3.1].

[c] Total quantum yield of visible and NIR emissions.

Table S2. Cole-Cole fitting for the parameter α.

T/K	**α (X_m')**	**α (X_m")**
2.0	0.2247	0.2375
2.5	0.2041	0.2316
3.0	0.2265	0.2393
3.5	0.2661	0.2634
4.0	0.2790	0.2823

Table S3. Crystallographic Data for Tb[3.3.1]

Chemical Formula	$TbGa_6C_{93.5}H_{99.5}N_{14.5}O_{27}$
Formula Weight	2435.61 g/mol
Crystal System, Space Group	Triclinic, $P\bar{1}$ (No. 2)
T	85(2) K
a	16.4342(3) Å
b	17.2269(3) Å
c	21.6881(4) Å
α	75.6312(16)°
β	70.7189(18)°
γ	89.4616(14)°
Volume	5596.7(2) $Å^3$
λ	1.54184 Å
ρ_{calc}	1.445 mg/m^3
Z	2
μ	5.254 mm^{-1}
F(000)	2458
θ range	2.235° to 73.947°
Limiting Indicies	$-20 < h < 20$
	$-21 < k < 21$
	$-26 < l < 24$
Reflections collected/unique	179289/22055
Completeness to θ	98.7%
No. of Data/Restraints/Params	22055/636/1493
GooF on F^2	1.051
[a]R_1	0.0472 [I>2σ(I)]; 0.0485 (all data)
[b]wR_2	0.1406 [I>2σ(I)]; 0.1426 (all data)
Largest Diff. Peak, Hole	1.422 e/$Å^3$; -1.687 e/$Å^3$

[a] $R_1 = \Sigma(||F_o|-|F_c||)/\Sigma|F_o|$ [b] $wR_2 = [\Sigma[w(F_o^2 - F_c^2)^2]/\Sigma[w(F_o)^2]]^{1/2}$; $w = 1/[\sigma^2(F_o^2) + (mp)^2 + np]$; $p = [\max(F_o^2,0) + 2F_c^2]/3$ (*m* and *n* are constants); $\sigma = [\Sigma[w(F_o^2 - F_c^2)^2/(n - p)]^{1/2}$

REFERENCES

(1) Chow, C. Y.; Eliseeva, S. V; Trivedi, E. R.; Nguyen, T. N.; Kampf, J. W.; Petoud, S.; Pecoraro, V. L. *J. Am. Chem. Soc.* **2016**, *138* (15), 5100–5109.